Journal of Inorganic Biochemistry 233 (2022) 111869

Contents lists available at ScienceDirect

Journal of Inorganic Biochemistry

journal homepage: www.elsevier.com/locate/jinorgbio

Structural insights into the design of reversible fluorescent probes for metallo-β-lactamases NDM-1, VIM-2, and IMP-1

Sky Price [a,1], Radhika Mehta [a,1], Dominique Tan [a], Abigail Hinojosa [a], Pei W. Thomas [b], Tawanda Cummings [a], Walter Fast [b], Emily L. Que [a,*]

[a] Department of Chemistry, University of Texas at Austin, 105 E 24th St Stop A5300, Austin, TX 78712, United States of America
[b] Division of Chemical Biology & Medicinal Chemistry, College of Pharmacy, and the LaMontagne Center for Infectious Disease, University of Texas at Austin, Austin, TX 78712, United States of America

ARTICLE INFO

Keywords:
Antibiotic resistance
Metalloenzyme inhibitor
Fluorescent probe

ABSTRACT

Metallo-β-lactamases (MBLs) are enzymes that are capable of hydrolyzing most β-lactam antibiotics and all clinically relevant carbapenems. We developed a library of reversible fluorescent turn-on probes that are designed to directly bind to the dizinc active site of these enzymes and can be used to study their dynamic metalation state and enzyme-inhibitor interactions. Structure-function relationships with regards to inhibitory strength and fluorescence turn-on response were evaluated for three representative MBLs.

1. Introduction

For the past century, antibiotics have revolutionized public health and saved millions of lives. However, despite the dramatic success of this innovation, numerous pathogens have developed a variety of resistance mechanisms. [1,2] This has led to a growing antibiotic resistance crisis: across the world, more than 700,000 patients lose their lives annually to drug-resistant infections. [3] The threat of multi-drug resistant pathogens is even greater in the Global South, where the infrastructure required to identify and combat multi-drug resistance is less developed. [4] Thus, there is an urgent need for our collective engagement with the threat of antibiotic resistance, especially to protect those communities that are most vulnerable to infectious disease.

One notable mechanism of resistance that has emerged in the past two decades is a new class of enzymes, β-lactamases, which catalyze the hydrolysis of the β-lactam ring in β-lactam-containing antibiotics. There are four different classes of these enzymes, of which three (classes A, C, and D) are serine β-lactamases whereas class B enzymes, metallo-β-lactamases (MBLs), require divalent metal ions such as Zn(II). Within the most clinically relevant B1 subgroup, these enzymes contain a dizinc active site and have an impressive substrate scope – they are capable of hydrolyzing nearly all β-lactam-containing antibiotics, including last-resort carbapenems. [5–7]

MBLs are rapidly evolving enzymes and their resistance genes are included in mobile plasmids in the form of gene cassettes, granting them the ability to horizontally transfer between bacteria. [6,8,9] In the mere decades that have passed since MBLs were first observed in pathogenic bacteria, they have been detected in dozens of countries around the world. [2,10] Moreover, MBL producers commonly have multiple additional drug resistances, which limits treatment options. [11] Accordingly, it is crucial to gain an increased understanding of these enzymes and the inhibitors needed to disable them. While there has been a great effort in the scientific community to develop inhibitors for these enzymes, there are none that are currently FDA-approved. [12]

We recently described [13] a reversible fluorescent probe, **DMAP-COOMe** (Fig. 1) that reversibly coordinates to the dizinc active site of one of the most prominent MBLs, New Delhi metallo-β-lactamase-1 (NDM-1). This probe consists of a solvatochromic fluorophore, 4-*N*,*N*-dimethylaminophthalimide (DMAP), coupled to a thiol-containing moiety, a widely-exploited group for MBL inhibition, [14] though limited in therapeutic applicability due to potential cross-reactivity with human metalloenzymes. [15] In the presence of NDM-1, the probe exhibits up to a 17-fold increase in fluorescence intensity suitable for live-cell imaging. Importantly, this probe can be displaced by either zinc chelation or active site inhibitors, making it potentially useful for the study of new antibiotic resistance therapies and nutritional immunity mechanisms.

Herein, we describe the development of a library of fluorescent

* Corresponding author.
E-mail address: emilyque@cm.utexas.edu (E.L. Que).
[1] Sky Price and Radhika Mehta should be listed as co-first authors as they made equal contributions.

https://doi.org/10.1016/j.jinorgbio.2022.111869
Received 10 February 2022; Received in revised form 10 May 2022; Accepted 17 May 2022
Available online 20 May 2022

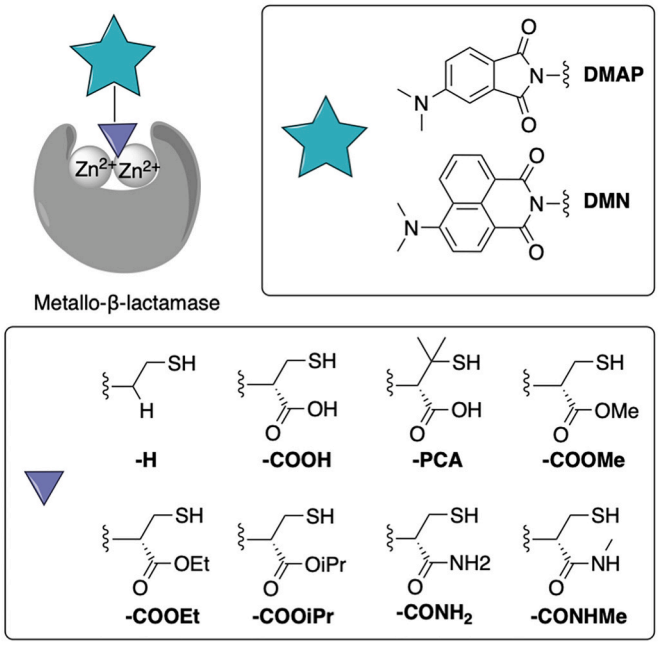

Fig. 1. Fluorescent probe library for metallo-β-lactamases including fluorophores (top box) and metal binding groups (bottom box).

probes related to **DMAP-COOMe** (Fig. 1) and investigate the effects of structural modifications on probe affinity and fluorescence turn-on response for NDM-1 and two other widespread MBLs: Verona integrin-encoded metallo-β-lactamase-2 (VIM-2) and imipenemase-1 (IMP-1). [16,17] Previously, we evaluated the interactions of probes **DMAP-H**, **DMAP-COOH**, and **DMAP-COOMe** with NDM-1. While **DMAP-COOH** produced the largest fluorescence turn-on, it exhibited only partial inhibition, and therefore **DMAP-COOMe** was chosen for further studies in bacteria. However, we found that **DMAP-COOMe** is rapidly processed by esterases in mammalian cells, and therefore would exhibit a large non-specific response when applied to host-pathogen studies. With this in mind, we designed probes that expanded upon this general scaffold by varying the ester moiety from methyl to ethyl and isopropyl esters, as well as substituting primary and secondary amides for the esters with the intention of slowing mammalian esterase activity or evading it entirely. These are commonly utilized strategies for reduction of esterase metabolism at metabolically vulnerable sites. [18] We also evaluated the impact of steric bulk directly adjacent to the metal-binding thiol by conjugating penicillamine to DMAP. Finally, we substituted a similar, bulkier fluorophore, 4-*N*,*N*-dimethylamino-1,8-naphthalimide (DMN), [19] with the three metal-binding groups originally reported (Fig. 1).

2. Materials and methods

2.1. Materials

All synthetic reagents were purchased from commercial sources and used without further purification unless otherwise noted. All reactions were run under N_2 atmosphere unless otherwise noted. All reverse-phase purification was performed using a Biotage Isolera One Flash Chromatography Instrument. NDM-1, VIM-2, and IMP-1 were expressed and purified as described previously. [20–22] Bovine carbonic anhydrase II and alkaline phosphatase were purchased from Sigma Aldrich. Phosphotriesterase was kindly provided by Prof. Frank Raushel from Texas A&M University. For all spectroscopic studies, 50 mM 4-(2-hydroxyethyl)-1-piperazineethanesulfonic acid (HEPES), pH 7.0 containing 10 μM $ZnSO_4$ was prepared as the buffer. ^{1}H and ^{13}C NMR spectra were recorded on a 400 MHz Agilent MR Spectrometer or a 400 MHz Bruker AVANCE NEO400 Spectrometer, prepared in deuterated acetonitrile, acetone, or methanol. The residual solvent peaks were used as an internal standard. Spectroscopic studies were performed using an Agilent Cary 60 UV–Vis spectrophotometer. Fluorescence spectroscopic measurements were made using an Agilent Cary Eclipse fluorescence spectrofluorometer. Confocal imaging was performed on a Zeiss 710 Laser Scanning Confocal Microscope. Data analysis was performed using GraphPad Prism Version 8.4.3.

2.2. Synthesis of compounds

Chromacef, [23] 4-*N*,*N*-dimethylaminophthalic anhydride, [24] and 4-*N*,*N*-dimethylamino-1,8-naphthalic anhydride [19] were synthesized according to literature procedures. **DMAP-H**, **DMAP-COOH**, and **DMAP-COOMe** were all synthesized according to the previously reported procedure. [13]

DMAP-COOEt. To a solution of **DMAP-COOH** (25 mg, 0.080 mmol) in ethanol (2 mL) at 0 °C under N_2 atmosphere was added thionyl chloride (100 μL, 1.40 mmol) dropwise. The reaction was allowed to reach room temperature, then was heated to reflux and left to react for 2.5 h. The volatile reagents were evaporated off, then the crude product was redissolved in 2:1 ethanol:H_2O (6 mL) and tris(2-carboxyethyl) phosphine (TCEP) (106 mg, 0.420 mmol) was added. The reaction was allowed to run overnight before the solvent was evaporated on a rotary evaporator, and the product was purified using reverse phase chromatography (50% MeCN/0.1% FA in H_2O) to yield the product as a yellow solid (17 mg, 0.050 mmol, 63% yield): ^{1}H NMR (400 MHz, CD_3CN) δ 7.65 (d, J = 8.57 Hz, 1H), 7.09 (d, J = 2.44 Hz, 1H), 6.94 (dd, J = 2.47, 8.58 Hz, 1H), 4.82 (dd, J = 5.12, 10.37 Hz, 1H), 4.14 (q, J = 7.35 Hz, 2H), 3.27 (m, 2H), 3.11 (s, 6H), 1.16 (t, J = 7.11 Hz, 3H) ppm; ^{13}C (100 MHz, CD_3CN) δ 169.3, 155.9, 135.2, 130.5, 125.8, 117.4, 116.2, 106.4, 62.7, 55.3, 40.7, 24.3, 14.3 ppm; HRMS ESI$^+$ *m/z* calc'd for $[C_{15}H_{18}N_2O_4S + H]^+$ (323.1064, observed; 323.1060, expected).

DMAP-COOiPr. To a solution of **DMAP-COOH** (15 mg, 0.050 mmol) in isopropyl alcohol (2 mL) at 0 °C under N_2 atmosphere was added thionyl chloride (100 μL, 1.40 mmol) dropwise. The reaction was allowed to reach room temperature, then was heated to reflux and left to react for 2 h. The volatile reagents were evaporated off, then the crude product was redissolved in 2:1 isopropyl alcohol:H_2O (6 mL) and TCEP (22 mg, 0.09 mmol) was added. The reaction was allowed to run for 72 h before the solvent was evaporated on a rotary evaporator, and the product was purified using reverse phase chromatography (60% MeCN/0.1% FA H_2O) to yield the product as a yellow solid (4.0 mg, 0.012 mmol, 23% yield): ^{1}H NMR (400 MHz, $(CD_3)_2CO$) δ 7.63 (d, J = 8.3 Hz, 1H), 7.07 (d, J = 2.4 Hz, 1H), 7.00 (dd, J = 8.5, 2.4 Hz, 1H), 4.99 (hept, J = 6.3 Hz, 1H), 4.83 (dd, J = 10.4, 5.1 Hz, 1H), 3.34 (m, 1H), 3.24 (m, 1H), 3.17 (s, 6H), 1.16 (dd, J = 19.4, 6.2 Hz, 6H) ppm; ^{13}C (100 MHz, CD_3CN) δ 169.2, 168.9, 168.6, 155.9, 135.3, 125.8, 117.4, 116.2, 106.4, 70.6, 55.5, 40.8, 24.4, 21.8 ppm; HRMS ESI$^+$ *m/z* calc'd for $[C_{16}H_{20}N_2O_4S + H]^+$ (337.1221, observed; 337.1217, expected).

DMAP-CONH$_2$. D-cysteine methyl ester hydrochloride (88 mg, 0.51 mmol) was placed in a vial that was then purged by vacuum and backfilled with N_2 gas 3×. Subsequently, ammonium hydroxide (1 mL) was added and the reaction was allowed to run at room temperature for 2.5 h before the solvent was evaporated off by high vacuum overnight. Separately, DMAP (30 mg, 0.15 mmol) was dissolved in acetic acid (3 mL); the flask was purged by vacuum and backfilled with N_2 gas several times. The resulting cysteine amide derivative was dissolved in methanol (0.5 mL) and transferred before the reaction was heated to 120 °C and allowed to run for 3 h. The solvent was evaporated by rotary evaporator and the crude mixture was purified by reverse phase chromatography (30% MeCN/50 mM NH_4OAC H_2O) to yield the product as a yellow solid (5.0 mg, 0.017 mmol, 11% yield): ^{1}H NMR (400 MHz, CD_3CN) δ 7.65 (dd, J = 0.42, 8.58 Hz, 1H), 7.10 (d, J = 2.39 Hz, 1H), 6.94 (dd, J = 2.46, 8.60 Hz, 1H), 6.42 (s, 1H), 5.84 (s, 1H), 4.69 (dd, J = 5.21, 10.54 Hz, 1H), 3.25 (m, 2H), 3.12 (s, 6H) ppm; ^{13}C NMR (100

MHz, CD_3CN) δ 170.8, 169.5, 155.9, 135.6, 125.7, 118.0, 116.2, 106.3, 56.4, 40.8, 24.4 ppm; HRMS ESI$^+$ *m/z* calc'd for $[C_{13}H_{15}N_3O_3S + H]^+$ (294.0913, observed; 294.0907, expected).

DMAP-CONHMe. D-cysteine methyl ester hydrochloride (88 mg, 0.51 mmol) was placed in a flask that was then purged by vacuum and backfilled with N_2 gas 3×. Subsequently, methylamine (1 mL) was added and the reaction was allowed to run at room temperature for 2.5 h before the solvent was evaporated off by high vacuum overnight. Separately, DMAP (29 mg, 0.15 mmol) was dissolved in acetic acid (3 mL); the flask was purged by vacuum and backfilled with N_2 gas several times. The resulting cysteine amide derivative was dissolved in methanol (0.5 mL) and transferred before the reaction was heated to 120 °C and allowed to run for 3 h. The solvent was evaporated by rotary evaporator and the crude mixture was purified by reverse phase chromatography (60% MeOH/50 mM NH_4OAC H_2O) to yield the product as a yellow solid (14 mg, 0.045 mmol, 29% yield): ^{1}H NMR (400 MHz, CD_3CN) δ 7.65 (d, J = 8.5 Hz, 1H), 7.10 (d, J = 2.5 Hz, 1H), 6.94 (dd, J = 8.6, 2.5 Hz, 1H), 6.60 (s, 1H), 4.66 (dd, J = 10.7, 5.1 Hz, 1H), 3.34 (m, 1H), 3.18 (m, 1H), 3.11 (s, 6H), 2.63 (d, J = 4.7 Hz, 3H) ppm; ^{13}C (100 MHz, CD_3CN) δ 168.9, 155.5, 135.1, 125.4, 117.3, 115.8, 105.9, 56.3, 40.4, 26.0, 24.0 ppm; HRMS ESI$^+$ *m/z* calc'd for $[C_{14}H_{17}N_3O_3S + Na]^+$ (330.0890, observed; 330.0883, expected).

DMAP-PCA. DMAP (105 mg, 0.520 mmol) and D-penicillamine (235 mg, 1.570 mmol) were dissolved in acetic acid (4 mL), the reaction was heated to 120 °C, and was left to react for 3 h. The solvent was evaporated by rotary evaporator and the product was purified by preparatory thin-layer chromatography (5% MeOH/DCM) to yield the product as a yellow solid (23 mg, 0.072 mmol, 14% yield): ^{1}H NMR (400 MHz, $(CD_3)_2CO$) δ 7.59 (d, J = 8.50 Hz, 1H), 7.06 (d, J = 2.37 Hz, 1H), 6.89 (dd, J = 2.38, 8.55 Hz, 1H), 3.08 (s, 6H), 1.88 (s, 3H), 1.61 (s, 3H) ppm; ^{13}C (100 MHz, CD_3OD) δ 170.8, 156.1, 135.8, 125.7, 118.3, 116.1, 106.4, 64.8, 40.5, 31.5, 30.8, 23.7 ppm; HRMS ESI+ *m/z* calc'd for $[C_{15}H_{18}N_2O_4S + Na]^+$ (345.0889, observed; 345.0879, expected). Note that one expected proton signal is missing from ^{1}H NMR; it is obscured by solvent peak at 4.84 ppm.

DMN-H. To a solution of DMN (51 mg, 0.21 mmol) in DMF (3 mL) was added pyridine (50 μL, 0.62 mmol), cysteamine (290 mg, 3.76 mmol), and 4 Å molecular sieves. The reaction was heated to 90 °C, then left to run overnight. The reaction mixture was then diluted with ethyl acetate (50 mL), washed with DI H_2O (3 × 10 mL) and brine (2 × 10 mL), then dried over sodium sulfate and concentrated by rotary evaporator. The crude residue was purified by reverse phase chromatography (70% MeCN/50 mM NH_4OAc H_2O) to yield the product as a yellow solid (12 mg, 0.040 mmol, 19% yield): ^{1}H NMR (400 MHz, CD_3CN) δ 8.49 (td, J = 1.19, 6.00 Hz, 2H), 8.38 (d, J = 8.25 Hz, 1H), 7.69 (dd, J = 7.31, 8.50 Hz, 1H), 7.17 (d, J = 8.29 Hz, 1H), 4.23 (m, 2H), 3.09 (s, 6H), 2.80 (m, 2H) ppm; ^{13}C (100 MHz, CD_3CN) δ 165.3, 164.6, 158.2, 133.3, 132.6, 131.6, 126.0, 125.9, 123.9, 118.3, 115.2, 114.2, 45.1, 43.5, 22.7 ppm; HRMS ESI$^+$ *m/z* calc'd for $[C_{16}H_{16}N_2O_2S + H]^+$ (301.1009, observed; 301.1005, expected).

DMN-COOH. To a solution of DMN (100 mg, 0.415 mmol) in DMF (5 mL) was added pyridine (100 μL, 1.24 mmol), COMU (355 mg, 0.829 mmol), D-cysteine (456 mg, 3.73 mmol), and 4 Å molecular sieves. The reaction was heated to 90 °C and allowed to proceed overnight before being diluted with ethyl acetate (50 mL), washed with DI H_2O (3 × 10 mL), and washed with brine (2 × 10 mL), then dried over sodium sulfate and concentrated by rotary evaporator. The crude residue was purified by reverse phase chromatography (30% MeCN/50 mM NH_4OAc H_2O) to yield the product as a yellow solid (44 mg, 0.13 mmol, 31% yield): ^{1}H NMR (400 MHz, MeOD) δ 8.70 (m, 2H), 8.61 (d, J = 8.61 Hz, 1H), 7.89 (t, J = 7.9 Hz, 1H), 7.39 (d, J = 8.3 Hz, 1H), 5.86 (dd, J = 9.9, 5.4 Hz, 1H), 5.18 (s, 6H), 3.72 (dd, J = 13.9, 5.4 Hz, 1H), 3.53 (m, 2H), 2.19 (d, J = 0.8 Hz, 3H) ppm; ^{13}C (100 MHz, CD_3CN) δ 176.2, 166.1, 165.6, 158.7, 134.0, 132.9, 132.1, 131.7, 126.3, 125.9, 124.1, 115.4, 114.2, 58.7, 45.0, 25.1 ppm; HRMS ESI$^+$ *m/z* calc'd for $[C_{17}H_{16}N_2O_4 + H]^+$ (345.0907, observed; 345.0904, expected).

DMN-COOMe. Acetyl chloride (20 μL, 0.28 mmol) was added dropwise to an oven-dried flask containing anhydrous methanol (20 mL) at 0 °C. After 30 min, **DMN-COOH** was transferred (25.6 mM in methanol, 5 mL) to the solution, and the reaction was left to run for 72 h. The solvent was evaporated by rotary evaporator and the crude residue was purified by reverse phase chromatography (70% MeOH/0.1% FA H_2O) to yield the product as a yellow solid (18.4 mg, 0.0510 mmol, 40% yield): ^{1}H NMR (400 MHz, CD_3CN) δ 8.55 (ddd, J = 14.1, 7.9, 1.2 Hz, 1H), 8.42 (d, J = 8.3 Hz, 1H), 7.73 (dd, J = 8.5, 7.3 Hz, 1H), 7.20 (d, J = 8.4 Hz, 1H), 5.80 (dd, J = 9.1, 5.6 Hz, 1H), 3.65 (s, 3H), 3.45 (m, 1H), 3.20 (m, 1H), 3.14 (s, 6H) ppm; ^{13}C (100 MHz, CD_3CN) δ 170.6, 165.1, 164.3, 158.7, 134.0, 133.3, 132.3, 131.4, 125.9, 125.8, 123.2, 114.1, 114.0, 56.1, 53.0, 45.1, 24.1 ppm; HRMS ESI$^+$ *m/z* calc'd for $[C_{18}H_{18}N_2O_4S + H]^+$ (359.1068, observed; 359.1060, expected).

2.3. Fluorometric titrations and selectivity studies

To a 10 μM solution of probe in 50 mM HEPES, pH 7.0 with 10 μM $ZnSO_4$ was added up to three equivalents of protein. For fluorometric titrations with NDM-1, VIM-2, and IMP-1, this was followed by an addition of 40 μM $ZnSO_4$ for a total volume of 105 μL. For selectivity studies with alkaline phosphatase, up to two equivalents of protein were added to a 2 μM solution of probe. Probe stock solutions were made in acetonitrile at either 2 mM or 4 mM concentration. All studies were conducted at room temperature with λ_{ex} = 420 nm and λ_{em} = 430–800 nm. Turn-on was calculated by integrating the area under each curve from 435 to 800 nm, subtracting the buffer baseline from all data, and then taking the ratio of fluorescence intensity for probe-protein *versus* the probe only. Each experiment was performed in triplicate, with the exception of values for **DMN-H,** all values for VIM-2, and all selectivity experiments, which were performed in duplicate if error bars are shown. The final fold-turn-on values after addition of 3 equiv. protein and supplementary $ZnSO_4$ were averaged. Values for **DMAP-COOMe** for NDM-1 were used as previously reported. [13]

2.4. Determination of IC_{50} values

IC_{50} values for each probe were determined for NDM-1, VIM-2, and IMP-1 using the colorimetric substrate chromacef. Assays were performed in 50 mM HEPES, pH 7.0 with 10 μM $ZnSO_4$, and organic solvent (acetonitrile or methanol) was kept at a constant 1% of assay volume. Additionally, 120 μM TCEP was included to decrease probe disulfide formation. Each reaction was performed with 50 nM protein and 25 μM substrate, with 8–14 probe concentrations varying between 0.015 and 32 μM for IMP-1, 0.03–64 μM for VIM-2, and 0.1–72 μM for NDM-1. Inhibitor and enzyme were pre-incubated for 26 min (750 μL) before the reaction was initiated by the addition of chromacef for a total assay volume of 1 mL. Absorbance at 442 nm was followed continuously for 0.5 min at room temperature, after which the slope of the linear portion (0.5 min for NDM-1, 0.1 min for IMP-1, VIM-2) was taken. The IC_{50} values were determined by plotting fractional activity *versus* probe concentration, where activity = 1 when no probe is added and the minimum activity is defined as Y = 0, with each value determined in triplicate. The resulting points were fit to a one-phase exponential decay on GraphPad Prism to determine the IC_{50}. These were then averaged between trials. See Figs. S9-S11.

2.5. Calculation of K_i values

For each IC_{50} value determined as described above, the average and standard deviation was converted to K_i assuming competitive inhibition according to the following equation:

$$K_i = \frac{IC_{50}}{1 + [S]/K_m}$$

where [S] was 25 μM for all trials, and K_m was 0.55 μM for NDM-1, [22] 8 μM for VIM-2, [25] and 4.8 μM for IMP-1. [26]

2.6. PLANTS docking simulations

Docking was carried out using v1.1 of PLANTS with the chemplp scoring function. The binding site center was defined as the coordinates of Zn2 with the binding site radius defined as 20 Å. Ten structures were generated for each run, with the cluster rmsd being set to 2.0. A distance constraint between the metal-binding thiol and each zinc ion was set (between 1.0 and 3.0 Å) where distances within this range add a weight of −3.0 to the score of the binding mode.

2.7. Evaluation of hydrolytic stability

Hydrolytic stability of the probes was evaluated by HPLC over 32 h, where the presence of the intact probe over time was monitored by peak area. A Kinetex C18 LC column (2.6 μm, 100 Å, 150 × 4.6 mm) was used to separate the intact ester from its hydrolysis product. The mobile phase was acetonitrile and water with 0.1% trifluoroacetic acid; a gradient from 10% acetonitrile to 90% acetonitrile was run over 8 min, then held at 90% acetonitrile for 2 min with a flow rate of 1.2 mL/min. The column temperature was set to 50 °C and the injection volume was 10 μL. The UV detector was set to monitor absorbance at 280 nm and all peak areas were determined from traces at this wavelength. Samples were prepared at 100 μg/mL concentration in either pH 2 or pH 11 aqueous solution, with 25% acetonitrile to keep the probes dissolved and equimolar TCEP to prevent disulfide formation. The samples were incubated at 40 °C for the duration of the experiment.

2.8. Cell culture

HeLa cell culture was performed in Dulbecco's modified Eagle's Medium (DMEM) containing 4000 mg/L glucose and sodium pyruvate, supplemented with 10% heat inactivated fetal bovine serum (FBS) and 1% antibiotics (200 U/cm^3 penicillin and 200 μg/cm^3 streptomycin) at 37 °C with 5% CO_2. For imaging, the cells were seeded onto ibidi 8-well μ-slides (0.3 mL capacity) and grown to 70% confluency prior to imaging.

2.9. Live cell imaging experiments

Live cell imaging was performed with Gibco live cell imaging medium at 37 °C. All studies were performed with λ_{ex} = 405 nm and λ_{em} = 486–614 nm with a 10 μM probe concentration. The overall organic solvent concentration was kept below 1% v/v, where an aliquot of probe stock in acetonitrile was added directly to the cell imaging medium. Staining was monitored for 10 min after the initial addition of the dye.

3. Results and discussion

3.1. Synthesis and characterization

In keeping with previous results, only the D isomer of each molecule was evaluated, as all three MBLs display preference for the D isomer of the thiol-based inhibitor captopril. [27] These MBL probes were synthesized in 1–3 steps in which cysteine or a cysteine derivative was conjugated to the anhydride precursor of either DMAP or DMN, followed by functional group modification as needed as described in the experimental section. Purity was confirmed by several analytical and spectroscopic techniques (see Supporting Information).

3.2. Inhibitory potency

We evaluated the inhibitory potency of each probe for NDM-1, VIM-2, and IMP-1 by measuring the rate of hydrolysis of the colorimetric substrate chromacef at varied probe concentrations. With each observed IC_{50} value, K_i was calculated assuming competitive inhibition and using substrate K_m values reported in the literature. [22,25,26] These data are reported in Table 1.

In general, the greatest inhibitory strength was observed for IMP-1, with nearly every probe displaying sub-micromolar affinity (Table 1). The inhibitory response for VIM-2 generally was slightly decreased, with statistically significant differences observed for the K_i values of **DMAP-COOiPr**, **DMAP-CONH$_2$**, **DMAP-CONHMe**, and **DMAP-COOH** (one-way ANOVA, $p < 0.05$). Comparatively, the K_i values recorded for each probe with NDM-1 were significantly larger (one-way ANOVA, $p < 0.0001$). It is not surprising that such a distinguishable difference in affinity is observed since D-captopril also exhibits a lower inhibitory potency for NDM-1 than VIM-2 or IMP-1. The hydrophobic active site of each enzyme, bounded by active site loop 3 (ASL3) and 10 (ASL10), varies in openness from the most open NDM-1 to least open IMP-1 (Fig. 2A-C). This structural variability contributes strongly to observed differences in substrate and inhibitor affinity. [27,28]

Within the probes containing the DMAP fluorophore, similar patterns of affinity were observed for all three proteins. Comparable inhibitory responses were observed for **DMAP-COOMe**, **DMAP-COOEt**, and **DMAP-COOiPr**, which confirms that change in steric bulk is well-tolerated by the enzymes' active sites. Intriguingly, there was no significant difference between the K_i values for the three ester probes for IMP-1, while for both NDM-1 and VIM-2, the bulkier **DMAP-COOiPr** exhibited a slight increase in K_i value.

While the K_i values for **DMAP-CONH$_2$** were higher than those of **DMAP-COOMe** and **DMAP-COOEt**, the affinity penalty is small enough that the probe could reasonably be applied in host-pathogen studies to evade mammalian esterases. In the case of NDM-1, docking studies performed using the program PLANTS [29] with residue positioning as modelled by quantum mechanical/discrete molecular dynamics (QM/DMD) simulations [13] show that the amide group interacts as a hydrogen-bond acceptor for a nearby lysine residue, similar to the ester group (Fig. S2). This is reflected by the K_i value for **DMAP-CONHMe**, which is more similar to those of the esters than is **DMAP-CONH$_2$**, implying that the hydrophobic methyl moiety interacts favorably with hydrophobic residues within the active site, such as His189.

For the probes containing the DMN fluorophore, affinity was largely

Table 1
IC_{50} and K_i values with standard deviation for all reported probes for NDM-1, VIM-2, and IMP-1.

	IC_{50} (μM)			K_i (nM)		
Compound	NDM-1	VIM-2	IMP-1	NDM-1	VIM-2	IMP-1
DMAP-H	12.9 ± 0.6	0.24 ± 0.05	0.47 ± 0.04	280 ± 10	60 ± 10	75 ± 6
DMAP-COOH	N/A[a]	1.26 ± 0.05	1.5 ± 0.2	N/A[a]	300 ± 10	240 ± 30
DMAP-COOMe	7.9 ± 0.8	0.18 ± 0.03	0.032 ± 0.005	170 ± 20	44 ± 7	5.2 ± 0.8
DMAP-COOEt	7.9 ± 0.6	0.13 ± 0.02	0.026 ± 0.003	170 ± 10	32 ± 5	4.2 ± 0.5
DMAP-COOiPr	10.3 ± 0.5	0.32 ± 0.05	0.035 ± 0.006	220 ± 10	80 ± 10	5.6 ± 1.0
DMAP-CONH$_2$	10.0 ± 0.7	1.7 ± 0.2	0.51 ± 0.07	220 ± 20	410 ± 50	80 ± 10
DMAP-CONHMe	8.2 ± 0.5	2.3 ± 0.2	0.48 ± 0.06	180 ± 10	560 ± 50	80 ± 10
DMAP-PCA	>150	>30	>50	>3000	>3000	>3000
DMN-H	2.4 ± 0.4	0.110 ± 0.004	0.23 ± 0.02	52 ± 9	27.0 ± 1.0	37 ± 3
DMN-COOH	N/A[a]	0.69 ± 0.05	1.02 ± 0.05	N/A[a]	170 ± 10	164 ± 8
DMN-COOMe	9.5 ± 0.6	0.41 ± 0.09	0.09 ± 0.01	200 ± 10	100 ± 20	15 ± 2

[a] Data not fitted due to observed partial inhibition.

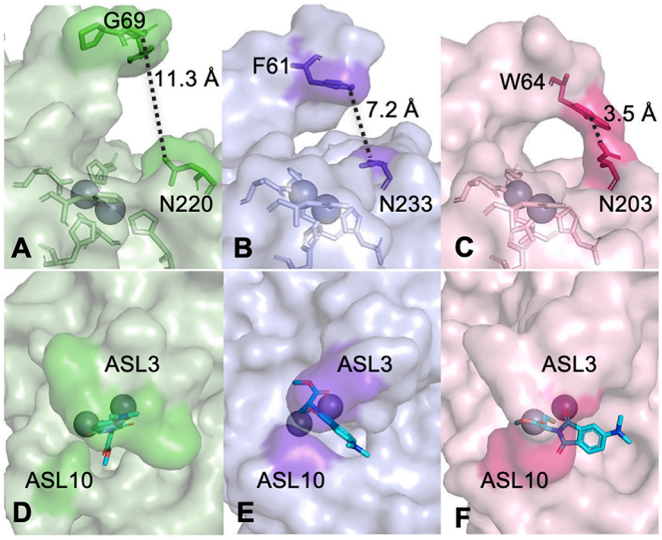

Fig. 2. (A-C) Side view comparison of active site approach for (A) NDM-1, (B) VIM-2, and (C) IMP-1 where the distance measured is that between active site loops 3 and 10 (ASL3 and ASL10). (D-F) Top view comparison of positioning of **DMAP-COOMe** (teal) in MBL active sites as modelled by PLANTS docking in (D) NDM-1, (E) VIM-2, and (F) IMP-1. PDB: 4EXS, 4C1D, 4C1F

retained in spite of the molecules' bulkier size. In particular, IMP-1 was able to bind both **DMN-H** and **DMN-COOMe** despite having the smallest active site among the enzymes (Fig. 2C), a result that is consistent with the broad substrate scope of the MBLs. For NDM-1 and VIM-2, but not IMP-1, **DMN-H** displayed smaller K_i values than **DMN-COOMe** in contrast to the DMAP fluorophore, where a methyl ester conferred greater inhibitory activity relative to the free thiol (Table 1). Given the more enclosed active site cavity of IMP-1, this observation is consistent with the greater overall hydrophobic surface area available to interact with hydrophobic substituents close to the metal-binding moiety.

The biggest similarity between the DMAP and DMN probe responses is between those of **DMAP-COOH** and **DMN-COOH**, which appeared to partially inhibit NDM-1 activity while retaining full inhibitory activity for both VIM-2 and IMP-1 (Table 1, Fig. S9–11). While **DMAP-COOH** and **DMN-COOH** inhibit VIM-2 and IMP-1 and approach 0% activity at increasing concentration, NDM-1 activity plateaus at a large non-zero value as the concentration of **DMAP-COOH** or **DMN-COOH** increases. Given these data, we hypothesize that the binding interactions made between NDM-1 and the carboxylic acid probes are different than the other probes such that the enzyme-probe complex is still able to turn over substrate to some degree, making **DMAP-COOH** and **DMN-COOH** partial inhibitors of NDM-1. [30] This phenomenon appears to be absent in VIM-2 and IMP-1.

Finally, poor inhibitory activity was observed for **DMAP-PCA** with all three MBLs (Table 1, Fig. S9–11). The two methyl groups adjacent to the thiol likely contribute enough steric strain such that it is unfavorable for the thiol to coordinate to the zinc ions within the active site. Additionally, the higher thiol pK_a of penicillamine (10.5) [31] relative to cysteine (8.6) [32] may contribute to decreased extent of deprotonation of the thiol at physiological pH and thus poor binding response.

3.3. Fluorescence response

In addition to the inhibitory capacity of these molecules, we evaluated their fluorescence response in the presence of all three MBLs by measuring the increase in fluorescence of 10 μM probe in the presence of increasing equivalents of protein (Fig. 3). Two buffer zinc concentrations (10 μM and 50 μM $ZnSO_4$) were tested to ensure that the MBLs were fully metalated under the assay conditions. A negligible change was observed upon zinc addition to the probe alone (Fig. S3), indicating that the baseline probe fluorescence is unaffected by the presence of zinc in the buffer.

Notably, there is no significant relationship between the K_i value of a probe and its associated fluorescence response. However, for all three proteins, the level of fluorescence increase observed for probes containing DMN is lower than those containing DMAP. This likely results from the DMN fluorophore being too large to be fully contained in the active site such that the hydrophobic ASL3 cannot fully shield the donor-acceptor junction of DMN from the bulk solvent.

The largest fluorescence response observed for NDM-1 (12.1-fold) in the presence of 10 μM $ZnSO_4$ was for **DMAP-COOMe**. With *in vitro* supplementation up to 50 μM $ZnSO_4$, turn-on was observed to increase to 17.0-fold. These results are consistent with those previously reported by our group. [13] For VIM-2, the highest fluorescence response (6.9-fold) was also observed for **DMAP-COOMe**. Supplementation of $ZnSO_4$ up to 50 μM resulted in an increase to 8.4-fold fluorescence turn-on. Finally, for IMP-1, the highest fluorescence response (7.4-fold) was observed for **DMAP-COOH**. Supplementation of $ZnSO_4$ up to 50 μM resulted in an increase to 8.6-fold fluorescence turn-on. As noted previously, the observed increase upon addition of zinc is indicative of the enzymes' lower affinity for binding at the Zn2 site compared to Zn1, and therefore more exogenous zinc is required to fully metalate the active sites under these conditions. [13] The greatest turn-on increase upon zinc supplementation was observed for NDM-1, in keeping with its lowest *in vitro* affinity for Zn(II) in the Zn2 site relative to VIM-2 and IMP-1. [22,25,28] The turn-on value upon zinc supplementation can be considered the maximum turn-on value for these proteins.

The three enzymes displayed the largest overall fluorescence

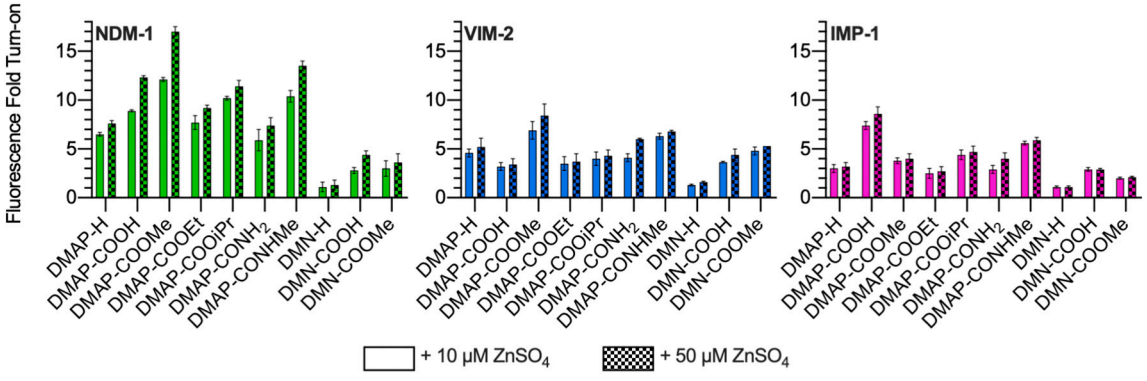

Fig. 3. Fluorescence fold turn-on for each probe (10 μM) with 3 equivalents NDM-1 (green), VIM-2 (blue), and IMP-1 (pink) in the presence of either 10 μM $ZnSO_4$ (non-patterned bars) or 50 μM $ZnSO_4$ (patterned bars). Error bars represent standard deviation. (For interpretation of the references to colour in this figure legend, the reader is referred to the web version of this article.)

response with a similar set of probes, albeit at different magnitudes. The conserved pharmacophore for fluorescence turn-on may mirror the shared ability of these enzymes to bind the conserved hydrophobic bicyclic β-lactam structure. Moreover, these results suggest the importance of hydrophobic interactions by the methyl group on **DMAP-COOMe** and **DMAP-CONHMe** and the isopropyl group of **DMAP-COOiPr** for positioning the fluorophore in a more hydrophobic environment. Additionally, it is interesting that **DMAP-COOH** exhibits such a large fluorescence response in NDM-1 despite its apparent partial inhibitory activity. In light of the similarly large response for IMP-1, the electronic interaction provided by a hydrogen-bond acceptor (either oxygen in the case of the esters or nitrogen in the case of the amides) is likely an important contributor to high fluorescence response. Indeed, a similar response is observed for **DMAP-COOMe** and **DMAP-CONHMe** such that the latter molecule could be readily substituted for purposes of greater compatibility with host-pathogen studies.

We evaluated the fluorescence selectivity of the probe library by incubating each probe with three other Zn(II)-dependent proteins: bovine carbonic anhydrase II (bCA), phosphotriesterase (PTE), and alkaline phosphatase (AKP). Of these proteins, PTE and AKP are dizinc enzymes and thus would be the most likely to yield off-target responses. With the exception of **DMAP-H** (9.6-fold) and **DMAP-CONH$_2$** (5.7-fold), no greater than ~2-fold increase in fluorescence was observed with bCA. Similarly, with AKP no greater than ~2.5-fold increase in fluorescence was observed. Incubation with PTE resulted in a $\geq$ 10-fold turn-on for all probes except **DMAP-COOH**, **DMAP-COOEt**, **DMN-H**, and **DMN-COOH** (Fig. S4). The largest fluorescence response observed (28-fold) was for **DMAP-CONH$_2$.** However, as discussed previously, [13] PTE is not found in the system where we perform our cell experiments (*E. coli*) and is instead primarily found in soil bacteria. [33] Thus, while the probes may not be completely selective for MBLs, they are selective in the biological context in which we have applied them. Further work is underway to replace the coordinating thiol group with a moiety that is more selective for MBLs.

3.4. Docking studies

Overall, NDM-1 displayed the highest-fold turn-on response for all probes tested, followed by VIM-2 and then by IMP-1, which rarely displayed greater than a 4-fold increase in fluorescence. Docking studies indicate that the fluorophore is exposed to the bulk solvent to differing extents as a result of the relative sizes of each enzyme's active site (Fig. 2D-F). These modelling results show that ASL3 of NDM-1 shelters the fluorophore from the bulk solvent (Fig. 2A, 2D), consistent with previous QM/DMD data (Fig. S5). [13] However, the less open ASL3 of VIM-2 (Fig. 2B, 2E) and especially of IMP-1 (Fig. 2C, 2F) forces the fluorophore to adopt a much more solvent-exposed position, thus resulting in a lower level of fluorescence. Alternatively, favorable interactions with hydrophobic residues within or surrounding the active site could be less accessible to the fluorophore for VIM-2 and IMP-1, contributing to the lower observed fluorescence response. This effect has also been postulated by Kurosaki et al., [34] who developed a solvatochromic probe for MBLs that conjugated a dansyl fluorophore to a multiple-carbon chain terminated by a thiocarboxylic acid. This molecule was observed to have a higher-fold turn-on for IMP-1 than for VIM-2 (10-fold and 6-fold, respectively) and the authors hypothesize that this difference is due to the substitution of Trp64 in IMP-1 for Ala64 in VIM-2. As this residue is substituted for Phe70 in NDM-1, one might expect an intermediate turn-on value for this enzyme according to this hypothesis.

3.5. Effects of modification of ester moiety

As mentioned above, one limitation of the **DMAP-COOMe** probe is a significant non-specific fluorescence response observed in mammalian cells, which we hypothesized was due at least in part to esterase catalyzed conversion of **DMAP-COOMe** to **DMAP-COOH**. We compared **DMAP-COOMe** to two representative probes, one with a bulkier ester moiety (**DMAP-COOiPr**) and one with an amide moiety (**DMAP-CONHMe**). We began by comparing aqueous hydrolysis rates of **DMAP-COOMe**, **DMAP-COOiPr**, and **DMAP-CONHMe** in both acidic (pH 2) and basic (pH 11) conditions (Fig. S6, Table S3). These data highlight the impact of the diminished electrophilic character of the bulkier isopropyl ester and secondary amide relative to the methyl ester, a trend that has been shown to decrease the rate of hydrolysis by mammalian esterases. [35] We then incubated mammalian cells (HeLa) with **DMAP-COOMe** and **DMAP-CONHMe**. Previous results showed a rapid and dramatic increase in fluorescence when **DMAP-COOMe** was incubated with MCF-7 cells, [13] and this result was recapitulated by our experiment in HeLa cells. Similarly, HeLa cells incubated with **DMAP-COOiPr** also displayed strong fluoresecence signal. Importantly, we observed negligible fluorescence when HeLa cells were incubated with **DMAP-CONHMe** under the same conditions (Fig. S7). Therefore, substitution of the methyl ester in **DMAP-COOMe** for a secondary amide in **DMAP-CONHMe** is a viable strategy for reducing non-specific fluorescence in mammalian cells.

4. Conclusions

We report the inhibitory activity and fluorescence turn-on response for a variety of analogues of a recently reported probe, **DMAP-COOMe**, a molecule capable of monitoring the dynamic metalation state of NDM-1 in *E. coli*. These factors are recorded for three MBLs: NDM-1, VIM-2, and IMP-1. There is no significant relationship observed between a given molecule's K_i value and its fluorescence turn-on response, but the probes clearly have greater affinity for VIM-2 and IMP-1 than for NDM-1, while exhibiting the greatest fluorescence turn-on in NDM-1 followed by VIM-2, and the least fluorescence turn-on in IMP-1. The greatest contributing factor to the observed trends in fluorescence response is the relative size of the active site approach for the three enzymes. Various other factors likely contribute including the relative positioning of hydrophobic residues within the active site. This result indicates that it should be feasible to generate a suite of turn-on fluorescent probes with varying affinities, which would be useful for gauging target interaction in competition with ligands that have a wide array of potency for binding the metallo-β-lactamase target (*e.g.* fragment screening or lead optimization). Additionally, substitution of the ester group for an amide yields a similar fluorescence response in NDM-1 but results in negligible fluorescence increase in mammalian cells, providing a potential avenue for greater compatibility with host-pathogen studies *via* a molecule lacking a hydrolyzable ester moiety. Future work will include exploration of the applications of this amide probe as well as modification of the sensor scaffold (including varying chain length between the fluorophore and metal binding group) with the goal of achieving improved fluorescence response in VIM-2 and IMP-1. The data presented within contribute to the understanding of the inhibitory properties of thiol-based probes for MBLs, and the effects of minor modifications near the metal-binding group. Additionally, the data provide insight into the development of selective reversible probes for MBLs that can be applied in inhibitor screening, in the hopes that clinically-effective inhibitors for these promiscuous enzymes can soon be developed.

Author contributions

S.P. and R.M. conceptualized and led the experiments and analysis. R.M., S.P., D.T., and A.H. synthesized and characterized the probes. S.P. performed the inhibition assays. S.P. and T.C. performed the fluorescence measurements. S.P. performed the docking experiments. S.P. performed the selectivity and hydrolytic stability experiments. S.P. performed the live cell imaging. P.W.T. expressed and purified proteins. W.F. provided input on experiments and analysis. E.L.Q. conceptualized the study and provided input on experiments and analysis. S.P. wrote the initial draft of the manuscript and all authors contributed to manuscript

editing and refinement.

Declaration of Competing Interest

There are no conflicts of interest to declare.

Acknowledgements

This work was supported in part by the National Institutes of Health (Grant R35 GM133612 to E.L.Q.; GM111926 to W.F.) and by the Robert A. Welch Foundation (Grant F-1883 to E.L.Q.; F-1572 to W.F.). T.C. received support for this work as a participant in the Chemical Research At Texas (CREATE) program funded by the National Science Foundation (Grant CHE-1945401 to E.L.Q.).

Appendix A. Supplementary data

Supplementary data to this article can be found online at https://doi.org/10.1016/j.jinorgbio.2022.111869.

References

[1] C.L. Ventola, P. T. 40 (2015) 277–283.
[2] P.M. Hawkey, A.M. Jones, J. Antimicrob. Chemother. 64 (2009) i3–i10.
[3] P. Dadgostar, Infect. Drug Resist. 12 (2019) 3903–3910.
[4] C.A. Hart, S. Kariuki, Br. Med. J. 317 (1998) 647–650.
[5] Y. Kim, M.A. Cunningham, J. Mire, C. Tesar, J. Sacchettini, A. Joachimiak, FASEB J. 27 (2013) 1917–1927.
[6] L. Poirel, T. Naas, D. Nicolas, L. Collet, S. Bellais, J.-D. Cavallo, P. Nordmann, Antimicrob. Agents Chemother. 44 (2000) 891–897.
[7] N. Laraki, N. Franceschini, G.M. Rossolini, P. Santucci, C. Meunier, E. de Pauw, G. Amicosante, J.M. Frère, M. Galleni, Antimicrob. Agents Chemother. 43 (1999) 902–906.
[8] N. Laraki, M. Galleni, I. Thamm, M.L. Riccio, G. Amicosante, J.M. Frère, G. M. Rossolini, Antimicrob. Agents Chemother. 43 (1999) 890–901.
[9] L. Poirel, L. Dortet, S. Bernabeu, P. Nordmann, Antimicrob. Agents Chemother. 55 (2011) 5403–5407.
[10] L. Dortet, L. Poirel, P. Nordmann, Biomed. Res. Int. 2014 (2014) 1–12.
[11] S.E. Boyd, D.M. Livermore, D.C. Hooper, W.W. Hope, Antimicrob. Agents Chemother. 64 (2020) e00397–20.
[12] N. Reddy, M. Shungube, P.I. Arvidsson, S. Baijnath, H.G. Kruger, T. Govender, T. Naicker, Expert Opin. Ther. Pat. 30 (2020) 541–555.
[13] R. Mehta, D.D. Rivera, D.J. Reilley, D. Tan, P.W. Thomas, A. Hinojosa, A. C. Stewart, Z. Cheng, C.A. Thomas, M.W. Crowder, A.N. Alexandrova, W. Fast, E. L. Que, J. Am. Chem. Soc. 143 (2021) 8314–8323.
[14] F.-M. Klingler, T.A. Wichelhaus, D. Frank, J. Cuesta-Bernal, J. El-Delik, H.F. Müller, H. Sjuts, S. Göttig, A. Koenigs, K.M. Pos, D. Pogoryelov, E. Proschak, J. Med. Chem. 58 (2015) 3626–3630.
[15] D. Büttner, J.S. Kramer, F.-M. Klingler, S.K. Wittmann, M.R. Hartmann, C.G. Kurz, D. Kohnhäuser, L. Weizel, A. Brüggerhoff, D. Frank, D. Steinhilber, T. A. Wichelhaus, D. Pogoryelov, E. Proschak, ACS Infect. Dis. 4 (2018) 360–372.
[16] L. Lauretti, M.L. Riccio, A. Mazzariol, G. Cornaglia, G. Amicosante, R. Fontana, G. M. Rossolini, Antimicrob. Agents Chemother. 43 (1999) 1584–1590.
[17] E. Osano, Y. Arakawa, R. Wacharotayankun, M. Ohta, T. Horii, H. Ito, F. Yoshimura, N. Kato, Antimicrob. Agents Chemother. 38 (1994) 71–78.
[18] T.N. Thompson, Med. Res. Rev. 21 (2001) 412–449.
[19] G. Loving, B. Imperiali, J. Am. Chem. Soc. 130 (2008) 13630–13638.
[20] Z. Cheng, C.R. Bethel, P.W. Thomas, B.A. Shurina, J.-P. Alao, C.A. Thomas, K. Yang, S.H. Marshall, H. Zhang, A.M. Sturgill, A.N. Kravats, R.C. Page, W. Fast, R. A. Bonomo, M.W. Crowder, Antimicrob. Agents Chemother. 65 (2021) e01714–e01720.
[21] Z. Cheng, B.A. Shurina, C.R. Bethel, P.W. Thomas, S.H. Marshall, C.A. Thomas, K. Yang, R.L. Kimble, J.S. Montgomery, M.G. Orischak, C.M. Miller, J. L. Tennenbaum, J.C. Nix, D.L. Tierney, W. Fast, R.A. Bonomo, R.C. Page, M. W. Crowder, MBio 10 (2019) e02412–e02419.
[22] Z. Cheng, P.W. Thomas, L. Ju, A. Bergstrom, K. Mason, D. Clayton, C. Miller, C. R. Bethel, J. VanPelt, D.L. Tierney, R.C. Page, R.A. Bonomo, W. Fast, M. W. Crowder, J. Biol. Chem. 293 (2018) 12606–12618.
[23] S. Yu, A. Vosbeek, K. Corbella, J. Severson, J. Schesser, L.D. Sutton, Anal. Biochem. 428 (2012) 96–98.
[24] M. Sainlos, B. Imperiali, Nat. Protoc. 2 (2007) 3201–3209.
[25] M. Aitha, A.R. Marts, A. Bergstrom, A.J. Møller, L. Moritz, L. Turner, J.C. Nix, R. A. Bonomo, R.C. Page, D.L. Tierney, M.W. Crowder, Biochemistry 53 (2014) 7321–7331.
[26] P. Oelschlaeger, M. Aitha, H. Yang, J.S. Kang, A.L. Zhang, E.M. Liu, J.D. Buynak, M.W. Crowder, Antimicrob. Agents Chemother. 59 (2015) 4326–4330.
[27] J. Brem, S.S. van Berkel, D. Zollman, S.Y. Lee, O. Gileadi, P.J. McHugh, T.R. Walsh, M.A. McDonough, C.J. Schofield, Antimicrob. Agents Chemother. 60 (2016) 142–150.
[28] M.F. Mojica, R.A. Bonomo, W. Fast, Curr. Drug Targets 17 (2016) 1029–1050.
[29] O. Korb, T. Stützle, T.E. Exner, Swarm. Intel. 1 (2007) 115–134.
[30] G.A. Grant, Arch. Biochem. Biophys. 653 (2018) 10–23.
[31] A. Al-Majed, F. Belal, S. Julkhuf, H. El-Subbagh, Profiles of Drug Substances, Excipients and Related Methodology, Elsevier, 2005, pp. 119–130.
[32] R.L. Thurlkill, G.R. Grimsley, J.M. Scholtz, C.N. Pace, Protein Sci. 15 (2006) 1214–1218.
[33] F.M. Raushel, H.M. Holden, in: D.L. Purich (Ed.), Advances in Enzymology - and Related Areas of Molecular Biology, John Wiley & Sons, Inc., Hoboken, NJ, USA, 2006, pp. 51–93.
[34] H. Kurosaki, Y. Yamaguchi, H. Yasuzawa, W. Jin, Y. Yamagata, Y. Arakawa, ChemMedChem 1 (2006) 969–972.
[35] T.L. Huang, A. Székács, T. Uematsu, E. Kuwano, A. Parkinson, B.D. Hammock, Pharm. Res. 10 (1993) 639–648.